Journal of Materials Chemistry A

Accepted Manuscript

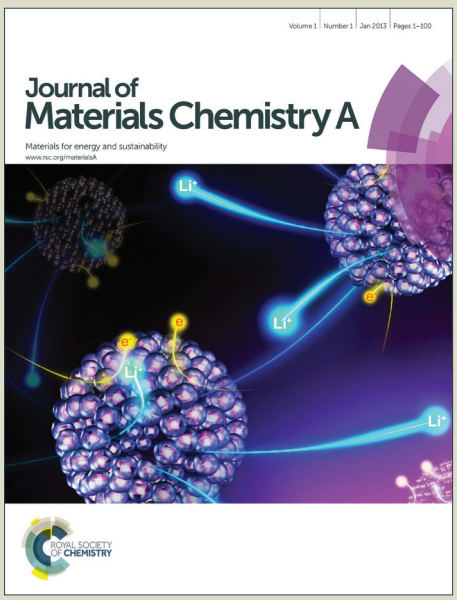

ROYAL SOCIETY OF CHEMISTRY

www.rsc.org/materialsA

Journal Name

RSCPublishing

ARTICLE

Microporous Titanate Nanofibers for Highly Efficient UV-Protective Transparent Coating

Cite this: DOI: 10.1039/xoxxoooooox

H. Hattori,[a] Y. Ide[b*] and T. Sano[a*]

Received ooth January 2012,
Accepted ooth January 2012

DOI: 10.1039/xoxxoooooox

www.rsc.org/

Hydrothermal treatment of a layered titanate ($K_2Ti_2O_5$) in the presence of tetrapropylammonium hydroxide and ammonium fluoride, inspired by a zeolite synthesis method called interzeolite conversion, produced a new titania-based material, a microporous titanate nanofiber. Judging from a variety of analyses such as high resolution transmission electron microscopy, Ar adsorption/desorption and adsorption of small and large cations from aqueous solutions, the product had several one-dimensional channels with a width less than 1 nm in a nanofiber. This new material showed a well-restrained photocatalytic activity, which was evaluated by the oxidation of cyclohexane and 2-propanol, and the activity was considerably lower than that of a photocatalytically inactive rutile-type TiO_2. The material also exhibited an extremely low refractive index (approximately 1.7). Thanks to these unique photoproperties, a microporous titanate nanofiber was successfully embedded in a commodity organic polymer (polycaprolactone) and then used as a highly efficient ultraviolet light (UV) protective transparent coating on a UV-sensitive substrate.

Introduction

UV produces DNA damage, immune suppression and skin photoaging, and is also responsible for the decomposition and degradation of organic compounds including plastics, polymers, dyes, pigments, wood and paper that compose most of modern commonly used articles and devices. Therefore, the protection against UV irradiation damage is of a great interest for ordinary people, scientists and industries. Organic UV absorbers, embedded in polymer coatings, have been extensively used to protect organic materials against UV irradiation by transforming the absorbed radiation energy into the less damaging thermal energy through photophysical processes.[1,2]

Due to its abundance, non-toxicity, high stabilities and UV-absorbing property, titania (and titanate) has been expected as the alternative to organic UV absorbers. However, titania presents major drawbacks to be used as UV absorbers: i) it exhibits a high UV-induced photocatalytic activity that can induce the photodegradation of organic media in which they are embedded; ii) it possesses a considerably higher refractive index than those of commodity polymer matrices, thus lowering the diffusion of visible light to whiten the medium (that limits its usage in color sensible applications, such as artwork protection and optical device). To overcome the drawbacks, development of new titania-based UV-absorbers has been actively investigated under size control of titania,[3] and its heteroelement doping[4] and hybridization with other inorganic semiconductors (e.g. cerium dioxide).[5] New non-titania inorganic UV absorbers have also been developed.[6,7]

In this article, we report the synthesis of a new titanate material, a microporous titanate nanofiber, by a new route inspired by a zeolite synthesis method. We demonstrate that the newly developed material effectively absorbs UV, hardly shows photocatalytic activity and exhibits an extremely low refractive index, and then can be applied to a highly efficient UV protective transparent coating

Experimental

Reagents and materials. TiO_2 (anatase), K_2CO_3 (99.9%), NH_4F (97.0%), $CaCl_2$ (>95%) and 2-propanol (99.5%) were purchased from Wako Pure Chemical Industry. Tetrapropylammonium (TPA) hydroxide (as a 40 wt% of aqueous solution), crystal violet (CV, >95.0%) and dodecylamine hydrochloride (>97.0%) were purchased from Tokyo Chemical Industry. Cyclohexane (99.7%) and acetonitrile (99.8%) were purchased from Nacalai Tesque. Rhodamine 101 and polycaprolactone (PCL) were obtained from Sigma-Aldrich. P25, rutile (JRC-TIO-06) and synthetic saponite were supplied by Nippon Aerosil, Catalysis Society of Japan and The Clay Science Society of Japan, respectively. TPA hydroxide was used after the evaporation of the solvent to tune a molar ratio of TPA and H_2O for hydrothermal reactions. All the other reagents and materials were used as received.

Hydrothermal reactions. $K_2Ti_2O_5$, prepared by a solid state reaction between K_2CO_3 and anatase according to the literature,[8] was mixed with TPA hydroxide, water and NH_4F at a molar ratio of $K_2Ti_2O_5$:TPA:H_2O:NH_4F = 1:0.8:5:0.2 in an Teflon-lined stainless steel autoclave, and the mixture was heated at 170 ^oC for a week. After the hydrothermal treatment, the dried gel-like solid was washed with water and dried at 70 ^oC to give the product and eluate. Control experiments were conducted without TPA hydroxide and/or NH_4F. P25 and $K_{0.66}Ti_{1.73}Li_{0.27}O_4$, which was prepared according to

the literature,[9] were also hydrothermally treated under the identical condition.

Characterization. The crystal morphology was observed by scanning electron microscopy (SEM, Hitachi S-4800) and elemental mapping of products was conducted by SEM and energy-dispersive X-ray (EDX) analysis. High resolution transmission electron microscopy (HRTEM) was performed with a JEOL JEM-3000F high-resolution transmission electron microscope equipped with EDX analyser. X-ray diffraction (XRD) patterns of the solid products were collected using a powder X-ray diffractometer (Bruker D8 Advance) with graphite monochromatized Cu Kα radiation at 40 kV and 30 mA. N_2 and Ar adsorption/desorption isotherms were obtained using a Belsorp-max apparatus (Bel Japan). Prior to the adsorption measurements, the samples were evacuated at 120 ^oC for 12 h. Infrared spectra were recorded using an FT-IR spectrometer (Nicolet 6700) with a resolution of 4 cm^{-1}. The sample was pressed into a self-supporting thin wafer, and then placed into a quartz cell equipped with CaF_2 windows. Prior to the measurements, the sample was evacuated at 200 ^oC for 3 h. Thermogravimetric-different thermal analysis (TG-DTA) curves were collected using a SSC/5200 apparatus (Seiko Instruments). The sample was heated from room temperature to 800 ^oC in an air flow (50 mL min^{-1}) at a rate of 10 ^oC min^{-1}. Inductively coupled plasma atomic emission spectroscopy (ICP-AES) was performed on a SPS 7700 plasma spectrometer (Seiko Instruments). Ultraviolet-visible (UV-vis) spectra were recorded with a JASCO V-579 UV/Vis/NIR spectrophotometer. X-ray photoelectron spectroscopy (XPS) was performed with a Kratos ESCA-3400 electron spectrometer, where the binding energies were calibrated by O 1s peak. Electrospray ionization (ESI) mass spectrum was recorded on a LCMS-8040 liquid chromatograph mass spectrometer (Shimadzu) in the negative ion mode at a desolvation temperature of 200 ^oC.

Ion exchange. 50 and 5 mg of MPTNF powders were mixed with an aqueous solution containing $CaCl_2$ (40 mL, 0.06-60 mmol L^{-1}) and CV (200 mL, 0.000875-0.0875 mmol L^{-1}), respectively, and the mixtures were stirred at room temperature for 3 days. The products were separated from the mixtures by centrifugation (3500 rpm, 15 min). The amounts of the adsorbed/desorbed Ca/K ions and the adsorbed CV ions were determined on the basis of ICP-AES and UV-vis spectroscopy, respectively, of the supernatants. For dodecylammonium adsorption, MPTNF (200 mg) was mixed with an aqueous solution containing dodecylammonium hydrochloride (100 mL, 19.4 mmol L^{-1}), and the mixture was stirred at room temperature for 6 h. The product was separated from the mixtures by centrifugation, and the amounts of the adsorbed dodecylammonium ions and the desorbed K ions were determined on the basis of TG curve of the recovered solid and ICP-AES of the supernatant, respectively

Photocatalysis. Sample (60 mg) and a solution of cyclohexane (2 mL) in O_2-saturated acetonitrile (18 mL) were added into a stainless-made closed container (75 mL) equipped with Pyrex glass window. The mixture was irradiated (λ > 320 nm) by a 1000 W m^{-2}-power solar simulator at room temperature, under shaking. After the irradiation, the head-space gas of the container was sampled to determine the amount of CO_2 evolved with gas chromatography (GC). After the removal of the powder by filtration, amounts of organic compounds in the supernatant were determined by GC. The oxidation of 2-propanol in water was conducted in a way similar to that conducted for cyclohexane oxidation.

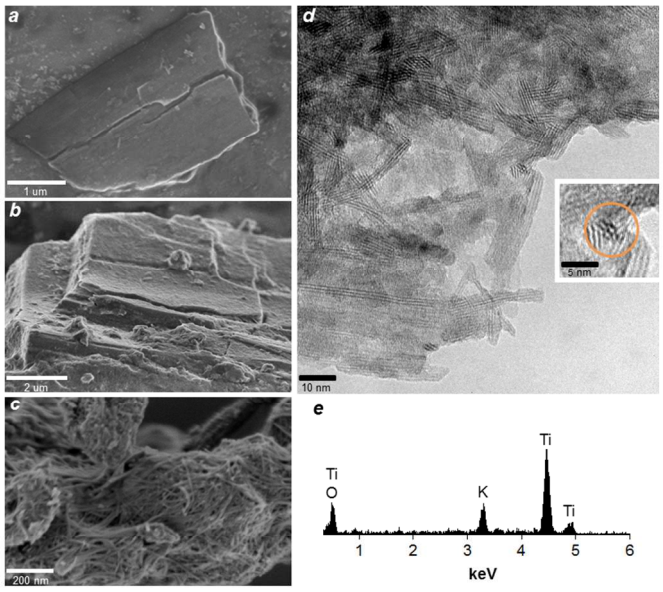

Fig. 1 (a and b) SEM images (a and b) of the starting $K_2Ti_2O_5$. (c) SEM image of MPTNF. (d) HRTEM image of MPTNF. Inset may show the edge view of a MPTNF particle. (e) EDX spectrum of MPTNF.

Preparation and evaluation of UV protective coatings. Rhodamine 101 film was prepared by casting a portion (2 mL) of a mixture of the dye (10.2 mol L^{-1}) and synthetic saponite (5.0 g L^{-1}) in an aqueous ethanol (30 mL, 1/1 in v/v) onto a glass substrate (28 mm-width and 48 mm-length) followed by evaporation of the solvent. A solution of polycaprolactone (200 mg) in chloroform (10 mL) was mixed with MPTNF or P25 (20 mg for each sample) and a portion (1.0 mL) of the mixture was casted onto the Rhodamine 101 film. After the evaporation of the solvent, the coated film was irradiated by 1000 W m^{-2}-power solar simulator (λ > 300 nm) at room temperature. Uncoated Rhodamine 101 film was also irradiated for comparison. The cast film of only MPTNF, P25 or $K_2Ti_2O_5$ embedded in polycaprolactone was also prepared on a quartz glass substrate to evaluate the transparency of the coating itself.

Results and discussion

The synthetic procedure of the present new titanate material was inspired by zeolite synthesis. Although the synthesis of zeolites, microporous aluminosilicates that have been widely used in industry, has traditionally been based on trial and error, more rational approaches are recently available. Of the approaches, the hydrothermal conversion of one zeolite into another, i.e. interzeolite conversion, has attracted increased attention.[10-12] In interzeolite conversion, one zeolite decompose into locally ordered aluminosilicate species (termed as "nanoparts"), whose structures are similar to the local structures of the original zeolite, and nanoparts assemble into another zeolite. In this study, we expanded the interzeolite conversion method, for the first time, to a layered titanate, $K_2Ti_2O_5$,[8] to design a new titanate material. We termed the product as "MPTNF" (microporous titanate nanofiber)". $K_2Ti_2O_5$ has a plate-like morphology with a lateral size of a few μm and a thickness up to several hundreds of nm (Fig. 1a and b) and is

composed of corrugated layers that are comprised of a distorted TiO_5 trigonal bipyramid and the interlayer K ions,[8] giving a basal spacing (multilayer repeat distance) of 0.64 nm (Fig. 2a). When the layered titanate was hydrothermally treated under an alkali condition in the presence of TPA hydroxide and NH_4F, which are often used in interzeolite conversion as a mineralizer and/or a structure-directing agent and a mineralizer, respectively, a product whose morphology and structure were different from those of $K_2Ti_2O_5$ was obtained. The product had a fibrous morphology with a diameter up to 10 nm and a length up to several hundreds of nm (so called "nanofiber") as can be seen in the SEM image and HRTEM image (Fig. 1c and d), showed a XRD pattern almost completely different from that of the starting $K_2Ti_2O_5$ (Fig. 2a) and exhibited abrupt N_2 uptake at lower partial pressure, which is indicative of the presence of micropores (a pore diameter < 2 nm) or microchannels, in the N_2 adsorption/desorption isotherms (Fig. 2b). Careful HRTEM observations revealed that neither nanotube-like particles nor small platy particles like $K_2Ti_2O_5$ fragments observed in Fig. 1a and b were not contained in the product at all, suggesting again that the product is microporous nanofibers derived from $K_2Ti_2O_5$.

EDX spectroscopy revealed the presence of O, K and Ti, and the absence of F in MPTNF (Fig. 1e), indicating that F was not incorporated in the product, or NH_4F acted as a mineralizer in the formation of MPTNF (this point will be described in detail below). We could not rule out the possibility of the occurrence of the only trace amount of F in MPTNF only from the EDX analysis; on the other hand, it is known that titania and titanate require substantial amounts of the incorporated F to slightly decrease the refractive indices[13] and then the amount of the incorporated F is negligible judging from the extremely low refractive index of MPTNF described below. The ICP-AES of the dissolved MPTNF determined the Ti and K contents (Ti, 42.1 wt%; K, 12.1 wt%). The TG-DTA curves of MPTNF did not show the weight loss due to the oxidative decomposition of TPA, confirming that TPA was not incorporated in the product; therefore, TPA hydroxide acted as a mineralizer rather than a structure directing agent (this point will be also described below). The TG-DTA curves also showed the weight loss (ca. 2.3 wt%) ascribable to the dehydration and condensation of the surface OH groups in a temperature range from 200 to 800 °C. The infrared spectrum of MPTNF shown in Fig. 2c confirmed the presence of isolated Ti-OH groups and hydrogen-bonded Ti-OH groups (peaks at 3721 and 3652 cm^{-1}, respectively). On the basis of Ti, K and OH contents, the chemical formula of MPTNF was calculated to be $H_{0.65}K_{0.75}Ti_{2.15}O_5$ (H exists as OH or partially H_2O; which will be described below).

We investigated the structure of MPTNF in more detail. When treated with an aqueous solution containing Ca ions, MPTNF adsorbed Ca ions accompanied by the desorption of K ions. As shown in Fig. 2d, the adsorption isotherm revealed the H-type adsorption according to the Giles classification,[14] which indicates strong interactions between MPTNF and Ca, and Ca adsorption capacity of ~ 2.3 mmol g^{-1}, which was comparable to the cation exchange capacity (1.75 mmol g^{-1}) of MPTNF for divalent cations predicted on the basis of the K content. These results indicate that K ions are located on the surfaces of the micropores or microchannels as exchangeable cations. A part of protons of the surface Ti-OH groups is also cation-exchangeable, judging from the fact that MPTNF could adsorb Ca ions more than the predicted cation exchange capacity. On the other hand, the adsorption of a cationic organic dye, crystal violet (CV; Fig. 2d inset) with a molecular size of 1.4 × 1.4 × 0.4 nm^3, from water on MPTNF was also the H-Type; however CV adsorbed considerably less effectively on MPTNF than Ca (Fig. 2d), implying that CV could not penetrate effectively along a nanofiber axial direction due to diffusion limitation. It should be noted here that the XRD pattern of MPTNF did not change significantly (e.g. the diffraction peak corresponding to the *d* value of 0.83 nm did not shift to a lower 2θ region) after the cation exchange reactions (similar phenomenon was

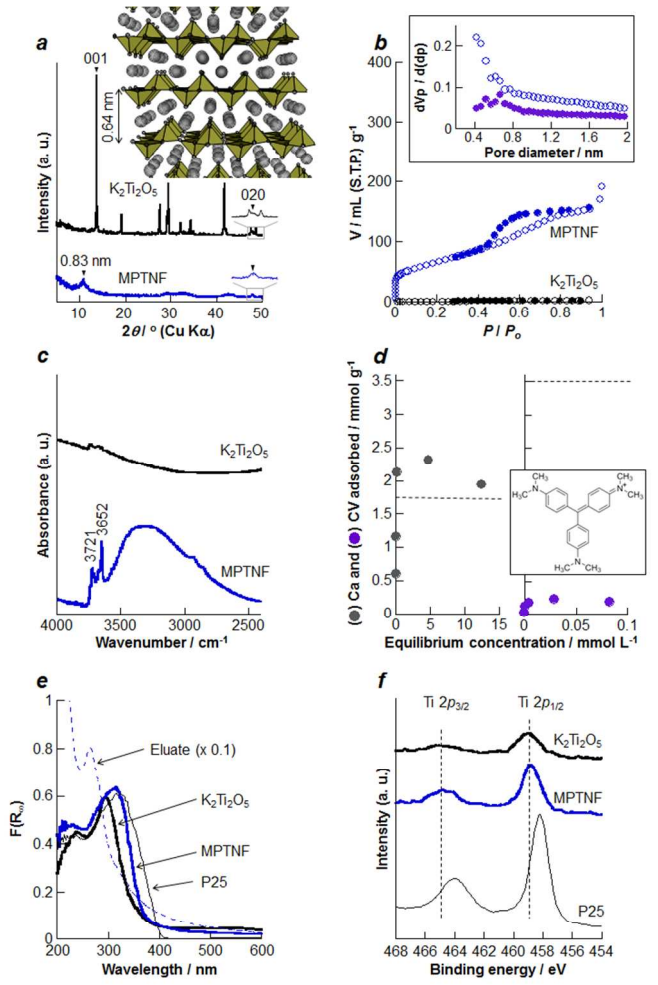

Fig. 2 (a) XRD patterns of $K_2Ti_2O_5$ and MPTNF. Inset shows the crystal structure of $K_2Ti_2O_5$ (grey spheres denote the interlayer K ions). (b) N_2 adsorption (open circles)/desorption (filled circles) isotherms of $K_2Ti_2O_5$ and MPTNF. Inset shows the pore size distribution of MPTNF (top) and the crystal violet (CV)-exchanged MPTNF (bottom) by Horwarth-Kawazoe method applied to the adsorption isotherms of Ar. (c) Infrared spectra of $K_2Ti_2O_5$ and MPTNF. (d) Adsorption isotherms of Ca (left) and CV (right) from water on MPTNF. Horizontal dashed lines denote the cation exchange capacity of MPTNF based on the K content for divalent and monovalent cations, respectively. Inset shows the structure of CV. (e) Diffused reflectance UV-vis spectrum of $K_2Ti_2O_5$, MPTNF and P25. UV-vis absorption spectrum of an eluate obtained during MPTNF synthesis is also shown. (f) Ti 2*p* XPS results of $K_2Ti_2O_5$, MPTNF and P25.

observed when K ions were almost quantitatively exchanged with dodecylammonium ions), supporting that MPTNF does not have a layered structure.[15] Horwarth-Kawazoe analysis,[16] which had successfully evaluated the microchannels (so called "tunnels" with a cross-section dimension of about 1.1 × 0.4 nm^2) of sepiolite that is a microfibrous silicate,[17] was applied to the treatment of the adsorption isotherms of Ar on MPTNF and the CV-exchanged MPTNF. From the analysis (Fig. 2b inset), MPTNF possessed a pore size distribution showing an effective pore diameter of ca. 0.5 nm and adsorbed a significantly smaller amount of Ar atoms after cation exchange with CV ions, which was explained by the fact that CV molecules inside (mainly in the vicinity of the particle outer surface of) MPTNF prevented the entrance of Ar atoms.[17] Such significant decrease of Ar uptake must not be observed if MPTNF has randomly oriented micropores or microchannels perpendicular to or across a nanofiber axial direction and similar phenomena have been observed for sepiolite[17] and zeolites with three-dimensional interconnecting microchannels.[18,19] Furthermore, as confirmed by the appearance of broad absorption at 3600-3000 cm^{-1} in the infrared spectrum measured after evacuation at 200 ^oC (Fig. 2c), significant amount of H_2O molecules adsorbed inside MPTNF, not but on the particle outer surface (thus a part of the surface OH groups are H_2O) and such phenomena have also been reported for sepiolite and zeolites. From the all results and facts described above, we deduce that MPTNF has one-dimensional microchannels rather than micropores. From the high micro pore volume up to 0.08 $cm^3\ g^{-1}$ (see below), that is comparable to that of sepiolite,[17] MPTNF presumably has a number of microchannels in a particle like sepiolite or TON-type zeolites. The expanded HRTEM image presented in Fig. 1d inset may show the edge of a MPTNF particle.

Besides its unique microstructure, MPTNF possessed i) a chemical stability toward water (acidic and basic solutions) and organic solvents, ii) an extraordinarily high cation exchange capacity (4.6 meq g^{-1} = 2 × 2.3 mmol g^{-1} for divalent cations) like a layered titanate, $H_2Ti_2O_5$, which is one of the most high-capacity (5.0 meq g^{-1}) cation exchangers among known materials but unstable in water[20] and iii) a fibrous morphology; therefore, it can be used as molecular sieve-like adsorbents, especially in chromatographic separations,[21] as well as UV absorbers.

We discussed the formation mechanism of MPTNF. After the hydrothermal reaction between $K_2Ti_2O_5$, TPA hydroxide, NH_4F and water, only dried gel-like product was recovered, and the product was washed with water to obtain MPTNF with a 76 % of yield on the basis of Ti content. On the other hand, the transparent eluate with water, which must contain 24 % of the added Ti, was also obtained. We thus thought that the eluate contained remnants of titania species (possibly "titania nanoparts") which assembled into MPTNF. In the UV-vis spectrum of the eluate, a sharp absorption peak centered at 270 nm, which was not appeared in the UV-vis spectrum of MPTNF, was observed (Fig. 2e). Zeolites or mesoporous silicas having isolated tetrahedral Ti species (highly dispersed titania species) show absorption at 220 nm in the UV-vis spectra.[22] While, in the UV-vis spectra for colloidal suspensions of titanate nanosheets derived from the exfoliation (delamination) of layered titanates, a well-developed absorption peak centered around 270 nm is often observed, which is explained by the presence of nanosheets with molecular-level thickness.[23,24] In the SEM image of the dried eluate, neither nanosheet-like particles derived from $K_2Ti_2O_5$ nor their ensembles were observed at all (only KOH particles with a size up to a few hundreds of nm were observed, although the corresponding SEM-EDX spectrum confirmed the presence of Ti, K and O). Also, in the XRD pattern of MPTNF, the (020) peak due to the diffraction within the titanate layers of $K_2Ti_2O_5$ was still observed (Fig. 2a). XPS revealed that MPTNF had unique five-coordinated Ti atoms like the starting $K_2Ti_2O_5$[8] although most titania and titanate, such as anatase and rutile (main components of a commercially available TiO_2, P25), had six-coordinated ones (Fig. 2f). Furthermore, the ESI-MS spectrometry, which had been applied to investigate speciation in silica and silicate solutions,[25,26] of the eluate showed the presence of a multitude of species up to approximately 400 Da (data not shown). Therefore, we thought that Ti species in the eluate were not Ti atoms derived from the complete dissolution of $K_2Ti_2O_5$, but "titania nanoparts" composed of TiO_5 trigonal bipyramid units (Fig. 2a, inset), whose molecular weight is much smaller than that of the exfoliated $K_2Ti_2O_5$ single-layer-nanosheet.

To understand the role of TPA and NH_4F in the formation of MPTNF, control hydrothermal reactions with or without the two compounds were conducted (Fig. 3). When neither TPA hydroxide nor NH_4F were added, split plate-like particles and bundled nanofibrous particles were predominantly obtained (Fig. 3a) and they possessed a poor crystallinity (Fig. 3b) and low mesopore (inter-particle pore) and micropore (intra-particle pore) volumes (Fig. 3c). By adding either TPA or NH_4F, well-defined nanofibrous products were obtained and they had a higher crystallinity than the product obtained in the absence of TPA and NH_4F; while, NH_4F gave a higher micropore volume product than did TPA. The addition of both TPA and NH_4F

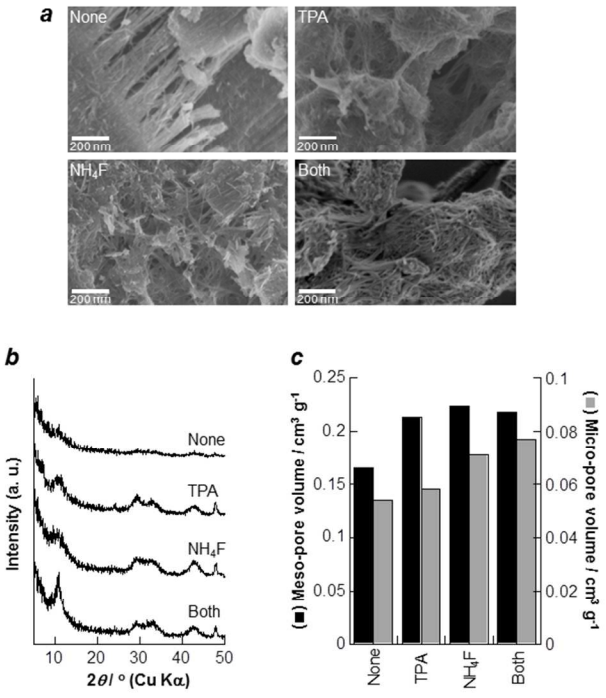

Fig. 3 (a) SEM images, (b) XRD patterns and (c) mesopore and micropore volumes, respectively, of hydrothermal products synthesized with and without TPA hydroxide and/or NH_4F. Mesopore and micropore volumes are determined by BJH method and from N_2 uptake at lower partial pressure, respectively.

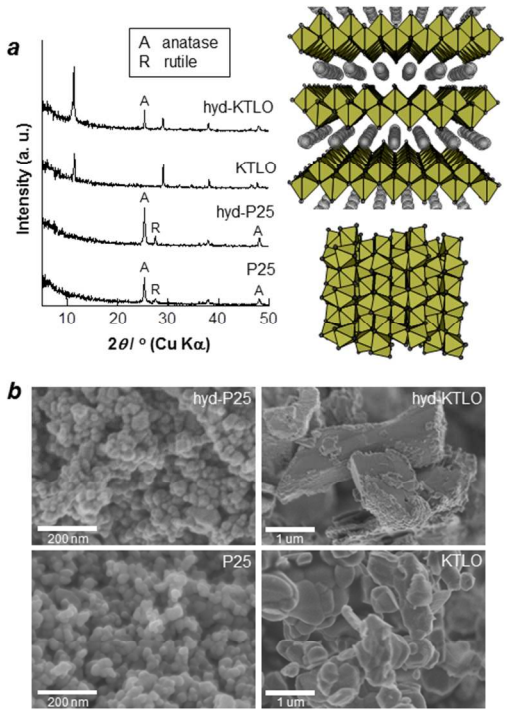

Fig. 4 (a) XRD patterns of P25 and $K_{0.66}Ti_{1.73}Li_{0.27}O_4$ (KTLO) and their hydrothermally treated products (hyd-P25 and hyd-KTLO, respectively). Inset show the crystal structures of rutile (bottom) and KTLO (top; grey spheres denote the interlayer K ions). (b) SEM images of P25, hyd-P25, KTLO and hyd-KTLO.

gave the best product (MPTNF) in terms of crystallinity and micropore volume, although the mesopore volume of MPTNF was similar to those for products obtained in the presence of TPA or NH_4F. From these results, both TPA and NH_4F promoted the decomposition of $K_2Ti_2O_5$ into titania nanoparts and NH_4F acted as a mineralizer to promote the assembling of the obtained titania nanoparts into MPTNF more effectively than TPA did.

It is well-known that TiO_2 (anatase, rutile, brookite or amorphous phase) can transform into titania nanotube under alkaline hydrothermal conditions (without any organic ammoniums and fluorides), and it is generally agreed that titania nanotubes form through the dissolution and subsequent recrystallization of TiO_2 particulate precursor into single- or multi-walled nanosheets, which then scroll or wrap into nanotubes.[27] Under the similar hydrothermal conditions at higher temperature, non-porous titania nanofibers (or nanorods) have also been obtained.[27] Furthermore, it has been reported that $K_2Ti_2O_5$ transforms into anatase (or TiO_2(B)) with a microfibrous morphology when treated with acid (cation-exchanged with proton) and then heated.[28-30] The XRD pattern of the present MPTNF was not in agreement with those of such conventional titania and titanate materials. These facts support our hypothesis that MPTNF forms through a new route involving the formation and assembling of titania nanoparts.

To further demonstrate our hypothesis, other inorganics were hydrothermally treated under the identical condition. After the hydrothermal treatment of P25 (composed of anatase, rutile and amorphous titania[31]), the intensity of the XRD diffraction peaks due to anatase and rutile increased (Fig. 4a) and smaller particles deposited on the original P25 particles (Fig. 4b), which were explained by the fact that amorphous titania converted into anatase and rutile. On the other hand, after the hydrothermal treatment of a layered titanate with lepidocrocite structure, $K_{0.66}Ti_{1.73}Li_{0.27}O_4$ (Fig. 4a inset),[9] anatase with a particle size less than 100 nm deposited on platy particles of the original titanate (Fig. 4a and b). This resulted from that amorphous phase or lower crystallinity-$K_{0.66}Ti_{1.73}Li_{0.27}O_4$ converted into anatase. Furthermore, a layered niobate, $K_4Nb_6O_{17}{\cdot}3H_2O$,[32] converted into a product whose structure and morphology were different from those of the starting niobates, nanotubular niobate (data not shown). Therefore, as reported for interzeolite conversion,[12] the local structures of starting materials is a key for the present hydrothermal conversion; it is difficult for anatase, rutile and $K_{0.66}Ti_{1.73}Li_{0.27}O_4$, in which TiO_6 octahedra are strongly connected each other by both point and edge shearing (Fig. 4a inset), to decompose into nanoparts under the present hydrothermal condition, on the other hand, $K_2Ti_2O_5$, amorphous titania (or lower crystallinity-$K_{0.66}Ti_{1.73}Li_{0.27}O_4$) and $K_4Nb_6O_{17}{\cdot}3H_2O$ possesses weakly connected TiO_5 trigonal bipyramids, TiO_6 and NbO_6 octahedra, respectively, each other only by point shearing and thereby can easily decompose into nanoparts. A wide variety of crystalline inorganics with different local structures is available and various hydrothermal conditions (higher temperature, stronger bases, structure directing agents, and so on) can be used; therefore, the presently proposed interzeolite conversion-inspired method seems versatile to design metal oxides nanostructured materials.

We investigated the photoproperties of MPTNF. Fig. 2e shows the UV-vis spectrum of MPTNF recorded in a diffused reflectance mode together with those of the starting $K_2Ti_2O_5$ and P25. The absorption onset (380 nm) of MPTNF was shifted to a longer wavelength region from that (345 nm) of $K_2Ti_2O_5$ (which is a merit of MPTNF as a UV absorber, because the most damaging natural UV radiation is between 290 nm and 350 nm[33]). It was noteworthy that MPTNF effectively absorbed UV like P25; therefore, we thought that analogous to P25 MPTNF showed a high photocatalytic activity when irradiated by UV. Fig. 5a shows the time-course change in the yield of products during the irradiation of simulated solar light ($\lambda > 320$ nm) to cyclohexane (CH) in the presence of dissolved O_2 over P25 or MPTNF. With P25, cyclohexanone (CHone) and cyclohexanol (CHnol), and a considerably larger amount of CO_2 formed. This resulted from that cyclohexyl radical, formed by the reduction of CH with either the valence band hole of P25 or hydroxyl radical derived from the reduction of OH^- with the valence band hole, was oxidized by oxidizing species such as the hydroxy radical and the superoxide anion, which was generated by the reduction of O_2 with the conduction band electron, to give CHone and CHnol that were easily overoxidized into CO_2.[34] On the contrary, MPTNF hardly gave even CO_2 and the products yield on MPTNF was considerably smaller even than rutile (JRC-TIO-06), one of the most inactive titanias for photocatalytic oxidations[35-37] (Fig. 5b). A similar tendency was observed for the photocatalytic oxidation of 2-propanol in water into acetone and CO_2 (data not shown). These results are worth mentioning as a merit of the present titanate, because the state-of-the-art titania nanostructures have exhibited higher photocatalytic activities than conventional titania (e.g. P25 with a surface area of ca. 50 $m^2\ g^{-1}$) due to some factors such as enhanced surface area. For example, titania nanotubes after calcination, with a surface area of ~150

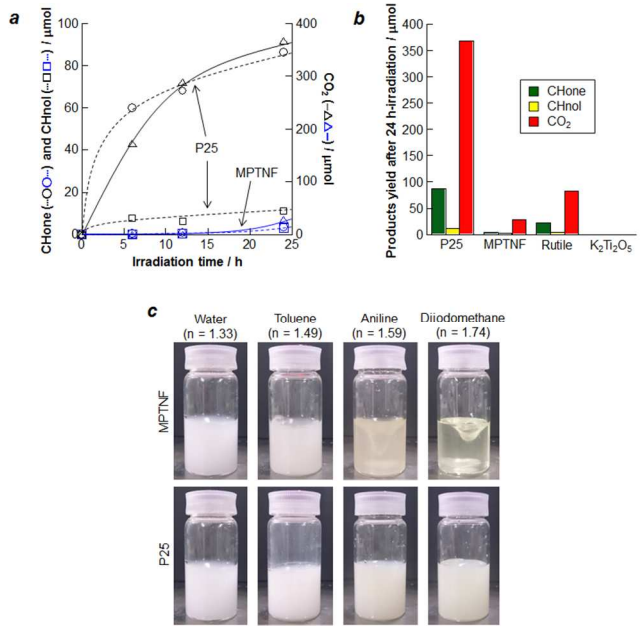

Fig. 5 (a) Time-course curves of photocatalytic oxidations of cyclohexane (CH) to cyclohexanone (CHone), cyclohexanol (CHnol) and CO_2 over P25 and MPTNF under simulated solar light irradiation ($\lambda > 320$ nm). (b) Yields of CHone, CHnol and CO_2 over P25, MPTNF, rutile and $K_2Ti_2O_5$ after the irradiation for 24 h. (c) Immersion tests to estimate the refractive index of MPTNF. 10 mg of powder samples are dispersed in 10 mL of organic solvents.

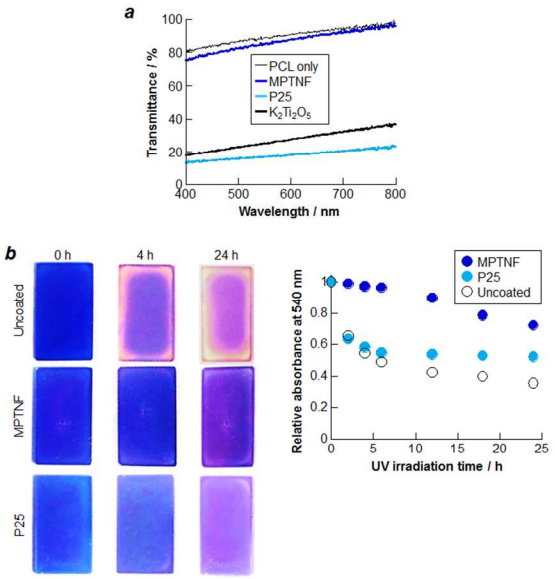

Fig. 6 (a) UV-vis transmittance spectra of films of PCL and those containing MPTNF, P25 or $K_2Ti_2O_5$. (b) Pictures showing Rhodamine 101 films uncoated and coated with MPTNF and P25 embedded in PCL before and after UV irradiation ($\lambda > 300$ nm). Inset shows time-course curves of the UV-induced photodegradation of the uncoated and coated Rhodamine 101 films.

m^2 g^{-1}, are effective UV-induced photocatalysts for the oxidation of various organic compounds (even as-synthesized titania nanotubes show significant photocatalytic activities).[38] The surface area (BET specific surface area) of MPTNF is up to 240 m^2 g^{-1} (*vs* < 1 m^2 g^{-1} for $K_2Ti_2O_5$), which is superior or comparable if compared to those of the state-of-the-art titania nanostructures. One possible reason for the low photocatalytic activity of MPTNF is the low crystallinity (Fig. 2a), since it is generally considered that titania with higher crystallinity (or lesser surface and bulk defects) shows higher photocatalytic activity for various reactions due to diminished electron-hole recombination rate.[39] Another possible reason is an inherent nature of $K_2Ti_2O_5$ nanoparts judging from the fact that the starting $K_2Ti_2O_5$ is almost inactive for the present photocatalytic reactions (Fig. 5b).

Due to its well-restrained photocatalytic activity for the complete oxidation of organic compounds into CO_2, MPTNF can be used as photocatalysts for partial oxidations of organic substrates,[40,41] after appropriate modifications such as calcination and metals deposition[42] and as fillers for organic resins,[43] as well as UV absorbers.

Another noticeable photoproperty of MPTNF is the extremely low refractive index. We used immersion method to determine the refractive index of MPTNF; the titanate powder (or P25 powder for reference) was dispersed in organic solvents with different refractive indices and the refractive index of the titanate was estimated by the transparencies of the dispersions observed with the naked eyes (Fig. 5c). P25 was opaque in the all solvents, which was explained by the fact that the refractive indices of anatase and rutile (2.53 and 2.71, respectively[44]) were much higher than those of organic solvents (as another possible reason, P25, whose primary particle size of 20-50 nm, aggregates in the solvents into larger-size particles to scatter visible light). However, MPTNF was almost transparent in diiodomethane having a refractive index of 1.74 (by "refractive index matching"), giving the estimated refractive index of 1.7. This value was considerably lower than those (2.4 ~ 2.7)[44] of conventional TiO_2. It has been established that the refractive indices (n) and density (d) of crystalline compounds obey the relationship, $(n-1)/d$ = constant,[45] and this formula has been found to work well for TiO_2.[44] Therefore, one plausible reason for such low refractive index of MPTNF is the low density due to the highly porous structure. MPTNF may also aggregate in organic solvents; however, the presence of mesopores between each nanofibrous particle may play a role in the lowering of the refractive index of the aggregate.

Thanks to the unique photoproperties described above, MPTNF was successfully used as a UV absorber embedded in a commodity organic polymer, polycaprolactone (PCL). In order to evaluate the UV protection ability of MPTNF, a highly UV-sensitive organic dye (Rhodamine 101) film and the same coated with PCL (having a refractive index of 1.53) in which MPTNF or P25 was embedded were irradiated by intense UV light ($\lambda > 300$ nm). The photodegradation of uncoated and coated Rhodamine 101 films was measured by monitoring their absorbance at 540 nm as a function of the irradiation time. As can be seen in Fig. 6a, MPTNF was successfully embedded in PCL to form a highly transparent film as a result of a small difference between refractive indices of MPTNF and PCL. When irradiated by UV light, Rhodamine 101 sample coated with the MPTNF film showed a substantial reduction of the photodegradation of the organic dye, being approximately 30

times slower than the uncoated sample (estimated by the initial slopes of Fig. 6b inset). On the contrary, P25, which has a much higher refractive index than that of PCL and a high photocatalytic activity, whitened the PCL matrix (Fig. 6a) and degraded the matrix and/or the organic dye immediately after the irradiation (Fig. 6b). $K_2Ti_2O_5$ could not be embedded homogeneously in PCL to form the whitened film (Fig. 6a), because the layered titanate did not swell or exfoliate (disperse at a nanometer level) in PCL and presumably had much higher refractive index[46] than PCL. All above results indicate that the presently developed MPTNF has the high potential for versatile and reliable UV-protecting materials. So far, titania has been widely applied in sunscreen products (mainly as UV blocking materials, not but UV absorbing ones). However, for such applications, titania is often required to restrain the high photocatalytic activity by the appropriate surface modification. Also, due to its high refractive index, titania loses transparency in the visible region, limiting the usage in applications requiring high transparency, such as optical devices, seriously.

Conclusions

We have reported that a layered titanate $K_2Ti_2O_5$ successfully converts into a new titanate nanostructured material, a microporous titanate nanofiber having possible one-dimensional multi-microchannels, via interzeolite conversion method. The new material exhibited a well-restrained photocatalytic activity and extremely low refractive index, which allowed us to create a highly efficient UV protective transparent coating on a UV-sensitive substrate. A wide variety of precursors (e.g. layered and microporous titanates[47]) with different compositions and local structures are available; therefore, the present synthetic strategy will make titania nanostructured materials' design much more attractive and versatile.

Notes and references

[a] Department of Applied Chemistry, Graduate School of Engineering, Hiroshima University, 1-4-1 Kagamiyama, Higashi-Hiroshima 739-8527, Japan.

[b] International Center for Materials Nanoarchitectonics (MANA), National institute for Materials Science (NIMS), 1-1 Namiki, Tsukuba, Ibaraki 305-0044, Japan.

1 J. Keck, M. Roessler, C. Schroeder, G. J. Stueber, F. Waiblinger, M. Stein, D. LeGourriérec, H. E. A. Kramer, H. Hoier, S. Henkel, P. Fischer, H. Port, T. Hirsch, G. Rytz and P. Hayoz, *J. Phys. Chem. B*, 1998, **102**, 6975.

2 M. Zayat, P. Garcia-Parejo and D. Levy, *Chem. Soc. Rev.*, 2007, **36**, 1270.

3 X. Chen and S. S. Mao, *Chem. Rev.*, 2007, **107**, 2891.

4 A. Demourgues, N. Penin, E. Durand, F. Weill, D. Dambournet, N. Viadere and A. Tressaud, *Chem. Mater.*, 2009, **21**, 1275.

5 H. Cui, M. Zayat, P. Garcia and D. Levy, *Adv. Mater.*, 2008, **20**, 65.

6 X. Wang, S. Zhou and L. Wu, *J. Mater. Chem. C*, 2013, **1**, 7547.

7 X. Wang, S. Zhou and L. Wu, *J. Mater. Chem. C*, 2014, **2**, 5752.

8 S. Andersson and A. D. Wadsley, *Nature*, 1960, **187**, 499.

9 Y. Fuse, Y. Ide and M. Ogawa, *Bull. Chem. Soc. Jpn.*, 2008, **81**, 767.

10 B. Subotić, D. Škrtić and I. Šmit, *J. Cryst. Growth*, 1980, **50**, 498.

11 H. Jon, N. Ikawa, Y. Oumi and T. Sano, *Chem. Mater.*, 2008, **20**, 4135.

12 K. Honda, M. Itakura, Y. Matsuura, A. Onda, Y. Ide, M. Sadakane and T. Sano, *J. Nanosci. Nanotechnol.*, 2013, **13**, 3020.

13 X. Rocquefelte, F. Goubin, Y. Montardi, N. Viadere, A. Demourgues, A. Tressaud, M.-H. Whangbo and S. Jobic, *Inorg. Chem.*, 2005, **44**, 3589.

14 C. H. Giles, T. H. Macewan, S. N. Nakhwa and D. Smith, *J. Chem. Soc.*, 1960, 3973.

15 T. Okada, Y. Ide and M. Ogawa, *Chem. Asian J.*, 2012, **7**, 1980.

16 G. Horvath and K. Kawazoe, *J. Chem. Eng. Jpn.*, 1983, **16**, 470.

17 E. Ruiz-Hitzky, *J. Mater. Chem.*, 2001, **11**, 86.

18 T. Takaishi, Y. Yatsurugi, A. Yusa and T. Kuratomi, *J. Chem. Soc. Faraday Trans. 1*, 1975, **71**, 97.

19 M. Niwa, S. Kato, T. Hattori and Y. Murakami, *J. Chem. Soc. Faraday Trans. 1*, 1984, **80**, 3135.

20 Y. Fujiki, Y. Komatsu, T. Sasaki and N. Ohta, *Nippon Kagaku Kaishi*, 1981, **10**, 1656.

21 T. Sasaki, Y. Komatsu and Y. Fujiki, *J. Radioanal. Nucl. Chem. Lett.*, 1986, **107**, 111.

22 F. Fan, Z. Feng and C. Li, *Acc. Chem. Res.*, 2010, **43**, 378.

23 T. Sasaki and M. Watanabe, *J. Phys. Chem. B,* 1997, **101**, 10159.

24 Y. Ide and M. Ogawa, *Chem. Commun.,* 2003, 1262.

25 S. A. Pelster, F. Schüth and W. Schrader, *Anal. Chem.*, 2007, **79**, 6005.

26 B. B. Schaack, W. Schrader and F. Schüth, *Angew. Chem. Int. Ed.*, 2008, **47**, 9092.

27 D. V. Bavykin, J. M. Friedrich and F. C. Walsh, *Adv. Mater.*, 2006, **18**, 2907.

28 M. He, X.-H. Lu, X. Feng, L. Yu and Z.-H. Yang, *Chem. Commun.*, 2004, 2202.

29 W. Li, C. Liu, Y. Zhou, Y. Bai, X. Feng, Z. Yang, L. Lu, X. Lu and K.-Y. Chan, *J. Phys. Chem. C*, 2008, **112**, 20539.

30 W. Li, Y. Bai, W. Liu, C. Liu, Z. Yang, X. Feng, X. Lu and K.-Y. Chan, *J. Mater. Chem.*, 2011, **21**, 6718.

31 T. Ohno, K. Sarukawa, K. Tokieda and M. Matsumura, *J. Catal.*, 2011, **203**, 82.

32 M. Gasperin and M.-T. le Bihan, *J. Solid State Chem.*, 1980, **33**, 83.

33 J. Pospíšil and S. Nešpurek, *Prog. Polym. Sci.*, 2000, **25**, 1261.

34 C. B. Almquist and P. Biswas, *Appl. Catal. A*, 2001, **214**, 259.

35 B. Ohtani, O. O. Prieto-Mahaney, D. Li and R. Abe, *J. Photochem. Photobiol. A*, 2010, **216**, 179.

36 D. Tsukamoto, Y. Shiraishi, Y. Sugano, S. Ichikawa, S. Tanaka and T. Hirai, *J. Am. Chem. Soc.*, 2012, **134**, 6309.

37 Y. Ide, H. Hattori and T. Sano, *Phys. Chem. Chem. Phys.*, 2014, **16**, 7913.

38 J. Suetake, A. Y. Nosaka, K. Hodouchi, H. Matsubara and Y. Nosaka, *J. Phys. Chem. C*, 2008, **112**, 18474.

39 H. Kominami, S. Murakami, J. Kato, Y. Kera and B. Ohtani, *J. Phys. Chem. B*, 2002, **106**, 10501.

40 Y. Shiraishi, N. Saito and T. Hirai, *J. Am. Chem. Soc.*, 2005, **127**, 12820.

41 Y. Ide, M. Torii and T. Sano, *J. Am. Chem. Soc.*, 2013, **135**, 11784.

42 Y. Ide, N. Kawamoto, Y. Bando, H. Hattori, M. Sadakane and T. Sano, *Chem. Commun.*, 2013, **49**, 3652.

43 Y. Fuse, Y. Ide and M. Ogawa, *Polym. Chem.*, 2010, **1**, 849.

44 X. Rocquefelte, F. Goubin, H.-J. Koo, M.-H. Whangbo and S. Jobic, *Inorg. Chem.*, 2004, **43**, 2246.

45 H. W. Jaffe, *Am. Mineral.*, 1956, **41**, 757.
46 T. Sasaki, Y. Ebina, T. Tanaka, M. Harada, M. Watanabe and G. Decher, *Chem. Mater.*, 2001, **13**, 4661.
47 Y. Ide, M. Sadakane, T. Sano and M. Ogawa, *J. Nanosci. Nanotechnol.*, **2014**, *14*, 2135.

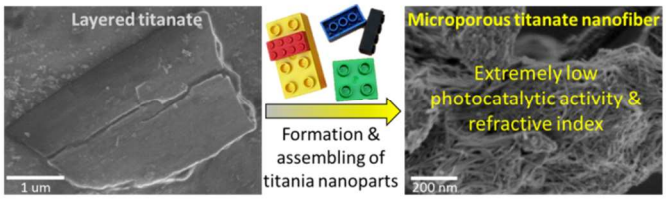

Interzeolite conversion was applied to convert a layered titanate into a microporous titanate nanofiber, which hardly showed photocatalytic activity and exhibited extremely low refractive index and then could be used as a UV absorber embedded in commodity organic polymer coating.